International Journal of Technology

http://ijtech.eng.ui.ac.id

Research Article

Structure and Electrochemical Corrosion Characteristics of Novel Single and Multilayer Nickel Aluminide based Composites

Leonid Agureev[1,2*], Svetlana Savushkina[1,2], Mikhail Gerasimov[3], Vasiliy Ignatenko[3]

[1]Keldysh Research Center, 125438 Moscow, Russia

[2]Moscow Aviation Institute (National Research University), 121552, Moscow, Russia

[3]Institute of Physical Chemistry and Electrochemistry of RAS, 119991 Moscow, Russia

[*]Corresponding author: trynano@gmail.com; Tel.:+7-903-723-79-69

Abstract: This study investigates NiAl-based composite materials produced by spark plasma sintering with various alloying additives (Cr, Co, Ti, Mo, V, Re, and Zr) and architectures (single-, two-, and three-layer configurations). The materials comprise an FCC solid solution matrix and regions with a mixed FCC–BCC structure containing large NiAl phase B2 intermetallic particles. The materials also contain the TCP phases of the Cr-Mo system (σ- and μ-phases). Electrochemical and corrosion studies were conducted in an aqueous solution (25 g/L CsCl + 11 g/L KCl + 9 g/L NaCl). The multilayer material NiAl-NiCrCoMoVReTiZr/NiCrCo/NiAlCoCrMoReTiZr exhibited the most favorable characteristics in terms of the ratio of current density in the passive state and the extent of the passive state region, namely, 299 mV and 0.0014 mA/cm^2. The most extended region of the passive state was found for the single-layer material NiAl-NiCrCoMoVReTiZr. However, its current densities in the passive state were higher (0.0033 mA/cm^2) versus 0.0013-0.0015 mA/cm^2 for other alloys. The lowest current density in the passive state was obtained for the NiAl-CrMoCoV material. Corrosion tests over a 6-month period revealed no mass changes or pitting traces in the material structure. This may be attributed to the chemical composition of the NiAl-based alloys, the presence of high-entropy regions, and the formation of intermetallic compounds, all of which enhance corrosion resistance.

Keywords: Composite material; Corrosion studies; Multilayer material; NiAl; Spark plasma sintering

1. Introduction

Multilayer alloys and composite materials are the subject of active research for modern energy systems, driven by the need to improve the operational durability of structural materials under extreme conditions. The structural organization of these materials ensures the maintenance of the required mechanical strength and operational safety in aggressive operating conditions, as they are resistant to degradation processes caused by high temperatures, corrosive agents, and ionizing radiation. These materials can provide corrosion resistance similar to that of precious metals while reducing production costs (Farihin et al., 2025; Rao et al., 2024; He et al., 2023; Grachev et al., 2020; Zhang et al., 2018; Perelygin et al., 2014).

Particular attention is being paid to multicomponent and high-entropy alloys (HEAs) that demonstrate excellent radiation resistance due to multilayer interfaces that contribute to the elimination of defects arising from irradiation. Thus, CrFeCoNi/TiNbZrTa, a HEA-based multilayer material, has shown increased resistance to heavy ion irradiation and corrosion (Rao et al., 2024; Zhang et al., 2018). Multilayer materials made of HEAs with nitride layers (AlTiCrNiTa)/(AlTiCrNiTa)N have demonstrated exceptional hardness, reaching 52 GPa, and high corrosion resistance even at elevated temperatures (He et al., 2023). The multilayer high-entropy

https://doi.org/10.14716/ijtech.v17i3.8279
Received December 2025; Revised January 2026; Accepted April 2026

structure of the materials improves adhesion and reduces residual stresses due to an increase in the number of interfaces between the layers, protecting it from both corrosion and mechanical damage under harsh operating conditions (Sasi et al., 2025; He et al., 2023).

NiAl-based β alloys are also of interest as a basis for heat-resistant structural materials with increased specific strength due to the high melting point of nickel aluminide (~1638 °C), a combination of high strength with low density, and also possessing high resistance to wear, corrosion, and creep under significant mechanical loads and elevated temperatures (Sun et al., 2025; Dikici et al., 2025; Agureev et al., 2022; Müller et al., 2021; Povarova et al., 2019; Xu et al., 2002). These properties are attributed to the strong interatomic Ni-Al bonds and ordered crystalline structure. A B2 crystal lattice (CsCl-type crystal lattice) characterizes NiAl. β-phase in the NiAl system is an ordered solid solution with an extensive homogeneity region. β-phase is in equilibrium with the γ'-phase (Ni_3Al) at temperatures below 1395 °C. In nickel-supersaturated solid solutions, this phase can undergo a martensitic transformation of the B2→ $L1_0$ type.

The alloying of the NiAl intermetallic compound with refractory metals (Cr, Mo, Re, V, and W) significantly improves its mechanical properties (Agureev et al., 2022). This process occurs through dispersion strengthening. The inclusion of the Häusler (e.g., Ni_2AlV) and Laves (e.g., Al_2V) phases creates effective barriers to dislocation movement. Directional solidification results in the formation of a unique eutectic microstructure by combining the NiAl matrix with secondary phase fibers or plates, which significantly increases fracture toughness by inhibiting cracks at phase boundaries (Lian et al., 2025; Feng et al., 2024; Wang et al., 2014 Kositsyn and Kositsyna, 2008). Alloying transition metals affects the diffusion kinetics. Thus, chromium replaces aluminum atoms, increasing the concentration of vacancies in the Al-rich region, accelerating aluminum diffusion and promoting the formation of a protective Al_2O_3 layer (Rizkia et al., 2015). Molybdenum substitutes for nickel, blocking vacancy migration paths in the Ni-rich region and reducing the nickel diffusion coefficient by an order of magnitude, increasing creep resistance (Romanovskaia et al., 2024; Henderson et al., 2021; Henderson et al., 2020; Ebrahimi et al., 2017; Zadorozne et al., 2010; Kositsyn and Kositsyna, 2008). Similar to nickel, cobalt participates in the triple defect, stabilizes the structure, and suppresses antisite formation. Vanadium in Al-rich compositions enhance CrMo phase solid-solution strengthening (Kositsyn and Kositsyna, 2008). The introduction of vanadium and chromium also reduces the concentration of defect clusters, thereby reducing brittleness and improving the ductility of the material. Studies (Jiang et al., 2025; Minamino et al., 2000) have established a direct relationship between NiAl composition, defect structure, and diffusion properties, which is especially important for the development of materials with improved thermal stability and corrosion resistance.

In this study, we investigated the structure and electrochemical corrosion characteristics of single-, two-, and three-layer nickel-aluminum-based composite materials produced by spark plasma sintering with different alloying additives.

2. Methods

2.1 Mixing and sintered

The following powders were used as initial materials: NiAl (PN70U30, 70 μm), Mo (1 μm), Co (less than 1 μm), Cr (PKh-1S, 140 μm), Ti (PTOM-1, 45 μm), vanadium granules (10 μm), Re (20 μm), and Zr (PTsRK, 60 μm). A mixture of NiAl-Cr, Mo, Co, and V powders was prepared so that the concentration of each element was in an equiatomic proportion to obtain base material 1. Mechanical alloying was performed using a vibratory mill and an Activator 2SL planetary mill. Mixing was performed in steel cups with the addition of a surfactant (0.5 wt. % oleic acid) using steel balls in a powder-to-balls ratio of 1:5 in a low vacuum. The duration of sequential mixing was 24 h in a vibratory mill and 2 h in a planetary mill. Table 1 presents the concentrations of various components and the characteristics of the resulting materials 1–4. We prepared multilayer materials by depositing slip films onto a pressed base from mixtures

of elements obtained similarly in the planetary mill. Single-layer and multilayer materials were consolidated by SPS using an FTC Systeme 025 setup at the Keldysh Research Center. The specimens were 30 mm in diameter and 3 mm in height. Hydrostatic weighing determined the density and porosity. Quanta 600 and Carl Zeiss Evo scanning electron microscopes (SEM) with X-ray spectral microanalysis systems (EDX) were used to study the structure and composition of the materials.

2.1.1 Corrosion tests

A solution (25 g/l CsCl + 11 g/l KCl + 9 g/l NaCl) was used as the model medium for the electrochemical and corrosion studies. The use of binary and ternary chloride melts for studying thermal storage media and MSRs motivates this choice. (Lambrecht et al., 2022). It is rational to use aqueous and solution models with chlorides at the preliminary material assessment stage. Cs is a common decay product in fuel systems (MSRs)/pyroprocessing and is incorporated into the salt as CsCl (or C halides). The behavior of Cs (volatility/solubility/reactions with the structural material) is critical for safety and corrosion (Beneš et al., 2021).

The samples were degreased and rinsed with distilled water. Electrochemical measurements were performed in a standard YSE-2 electrochemical cell using an IPC-PRO digital potentiostat-galvanostat (Volta, Russia). A platinum electrode was used as an auxiliary electrode, and a silver chloride electrode was used as a reference electrode. All potential values are given relative to the working solution's reversible hydrogen electrode. The solution temperature was maintained using a UTU-2 thermostat. Electrochemical tests were performed at a temperature of 25°C. The corrosion rate was studied after exposure to a solution (25 g/L CsCl + 11 g/L KCl + 9 g/L NaCl) for 6 months in aerated vessels by weighing the samples with an accuracy of 10^{-4} g. The samples were removed, dried, weighed, and re-immersed in the solution.

Table 1 Composition of the prepared samples

№	Composition (wt.%)	Properties
1	25NiAl-15Cr28Mo17Co15V	Base, single-layer
2	21NiAl-22Ni22Cr21.5Co3Mo7V0.4Re3Ti1Zr	Single-layer
3	21NiAl-22Ni22Cr21.5Co3Mo7V0.4Re3Ti1Zr // 34.7Ni30.6Cr34.7Co (upper layer, 200 μm)	Double-layer
4	21NiAl-22Ni22Cr21.5Co3Mo7V0.4Re3Ti1Zr // 34.7Ni30.6Cr34.7Co (middle layer, 200 μm)// Ni4Al9Co8Cr15Mo30Re7Ti15Zr (upper layer, 200 μm)	Triple-layer

3. Results and Discussion

3.1 Structure and composition

Figure 1a shows the microstructure of the NiAl-CrMoCoV base material. It consists of an FCC solid solution matrix and regions with a mixed FCC-BCC structure containing large particles of the NiAl phase-based B2 intermetallic compound. Lamellar phases interspersed with nanoscale clusters and submicron spherical phases are visible. The TCP phases are characterized by a lamellar shape. The lamellar formations are several microns long. Figure 1b shows the EDX mapping results. Overall, the elements are distributed fairly uniformly, which is typical of high-entropy materials. Iron is also present as an impurity. Nickel and impurity iron have elevated concentrations in some map areas. Table 2 presents the surface layer composition according to EDX.

The density of the sintered NiAl-CrMoCoV material was 7.09 g/cm^3, and the total porosity was 0.6%, as determined by hydrostatic weighing. According to the element distribution map, the material contains regions enriched to varying degrees in NiAlCo-, CrMoV-, and NiAlCo-containing phases. NiAl–Cr is a compound of B2-type NiAl(Cr) solid solutions and BCC Cr

as the second phase. The introduction of molybdenum into the NiAl–Cr system precipitates secondary phases. The σ-phase of CrMo and various intermetallic compounds of the Ni-Al-Mo type can be distinguished. Simultaneously, molybdenum exhibits high solubility in the BCC structure of chromium, where the formation of solid solutions or ordered phases with a concentration of up to 20-30 at.% is possible, including the formation of the σ-phase of CrMo. Cobalt exhibits high solubility in the intermetallic compound NiAl, reaching 15-20 at.%. Cobalt can effectively replace nickel atoms in the B2 structure while maintaining crystal lattice stability.

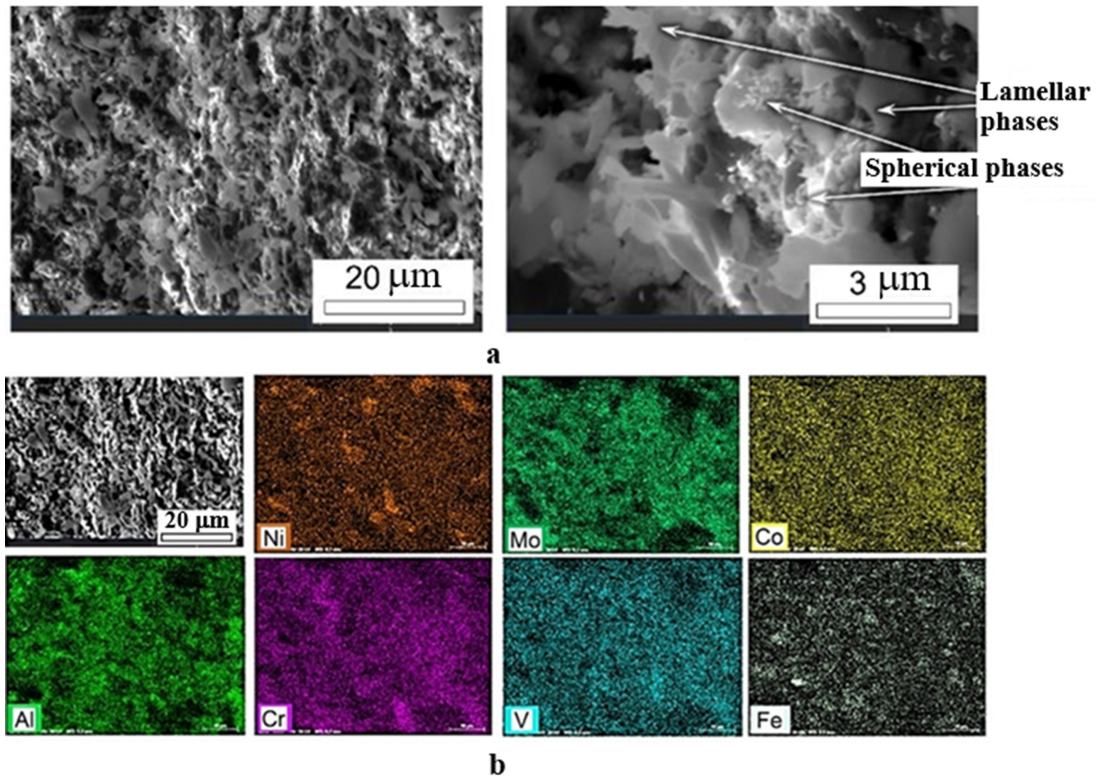

Figure 1 (a) SEM images of the microstructure of the sintered material 1 and (b) a map of the element distribution according to the EDX mapping spectral microanalysis data

Table 2 Surface layer composition according to EDX for all samples

№	Ni, at.%	Al, at.%	Cr, at.%	Co, at.%	Mo, at.%	Fe, at.%	V, at.%	Ti, at.%	Zr, at.%	Re, at.%	Ni/Al	Ni/Cr
1	17.3	19.0	43.0	2.5	3.3	3.8	11.0	-	-	-	0.9	0.4
2	15.9	8.9	38.2	8.6	6.6	2.3	13.5	2.3	2.5	1.2	1.7	0.4
3	44.9	3.6	22.5	18.0	6.8	2.9	1.5	0.4	0.9	-	12.4	1.9
4	15.0	8.9	14.3	10.4	10.3	1.7	-	13.4	13.3	12.7	1.7	1.0

According to X-ray phase analysis and thermodynamic modeling with J-MatPro (Agureev et al., 2025), the material contains BCC, FCC solid solutions, NiAl, and TCP phases, presumably representing σ- and μ-phases based on the Cr-Mo system. A special type of crystalline packing of atoms characterizes these phases and increases their heat resistance. However, in specific cases, corrosion resistance can be both worsened and improved by slowing down diffusion processes. The bending strength of base material 1 at room temperature and elevated temperatures (750, 900, and 1200 °C) was 760, 723, 694, and 100 MPa, respectively (Agureev et al., 2025).

One modification of the NiAl-CrMoCoV system may be a powder composite based on the NiAl-NiCrMoCoVReTiZr system (2). Here, the addition of Re, Ti, and Zr contributes to improved strength and creep resistance. The microstructure consists of elongated or vermicular grains with a diameter of approximately units of micron or less, interspersed with a second

phase in the form of thin streaks. (Figure 2 a, b). According to the EDX map, the material contains areas enriched to varying degrees in Ni and Co; Cr, Mo, and V; Cr, V, and Ti, Re, Al, Zr, Al, Cr, and Ti- containing phases (Figure 2, c). The phase composition calculation showed a complex BCC solid solution, NiAl, σ, γ' as the main phases. The Ni/Al ratio in the surface material layer increased, whereas the Ni/Cr ratio remained unchanged compared to material 1 (Table 2). The addition of Zr led to the formation of Al- and Zr-based phases, which can be assumed to be Al_3Zr (dark elliptical areas in Figure 2b). The solubility of V in NiAl is limited to 5-10 at.% at equilibrium. The material may contain secondary phases such as Al_8V_5, as well as the ternary intermetallic compounds involving Cr and Mo at this V concentration. In the BCC lattices of Cr and Mo, the solubility of V increases to 15–20 at.%, which is explained by the isomorphism of the crystal structures (BCC for V, Cr, and Mo) and the proximity of the lattice parameters (Agureev et al., 2025; Fu et al., 2013).

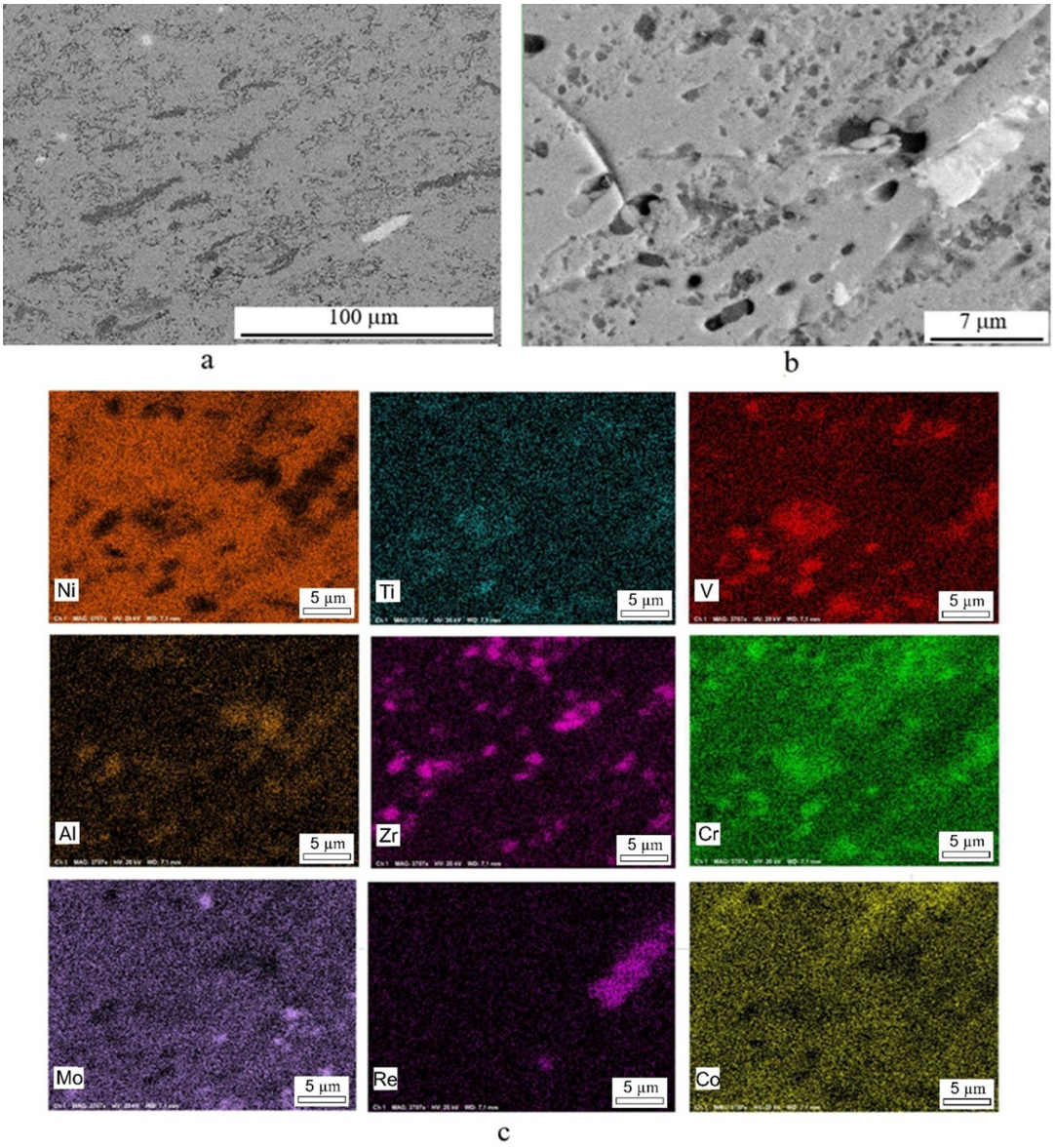

Figure 2 (a, b) SEM images of the microstructure of sintered material 2 at different magnifications and (c) a map of the element distribution according to X-ray spectral microanalysis data

Figure 3 shows the microstructure of the multilayer materials 3 and 4. The materials consist of alternating layers that differ in composition and structure. The bottom layer (substrate) corresponds to material 2. The inner layer of the two-layer material NiAl-

NiCrCoTiMoVReZr/NiCrCo is enriched with chromium. The Zr- and Re-containing phases are also noticeable (Figure 3 a, b). The EDX mapping revealed inner-layer elements, such as Al, Mo, V, Ti, and Zr, in the upper NiCrCo layer. This is due to the intense diffusion processes that occur during spark plasma sintering. Cr, Mo, and V; Al, and Ti-enriched areas are visible in the cross-section of the layer (Figure 3 b).

The three-layer material contains a top layer of Ni4Al9Co8Cr15Mo30Re7Ti15Zr, approximately 200 m thick (Figure 3, c). Its microstructure is a mixture of elongated or vermicular micron and submicron grains with a second phase in the form of thin streaks (micron or less wide) between them. The elongated white grains represent the Re-, Cr-, and Mo-based phases. Light gray areas correspond to the Ti-, Cr-, and Ni-containing phases, while dark gray areas correspond to the phase with a high zirconium content. Cobalt is uniformly distributed (Figure 3d, e).

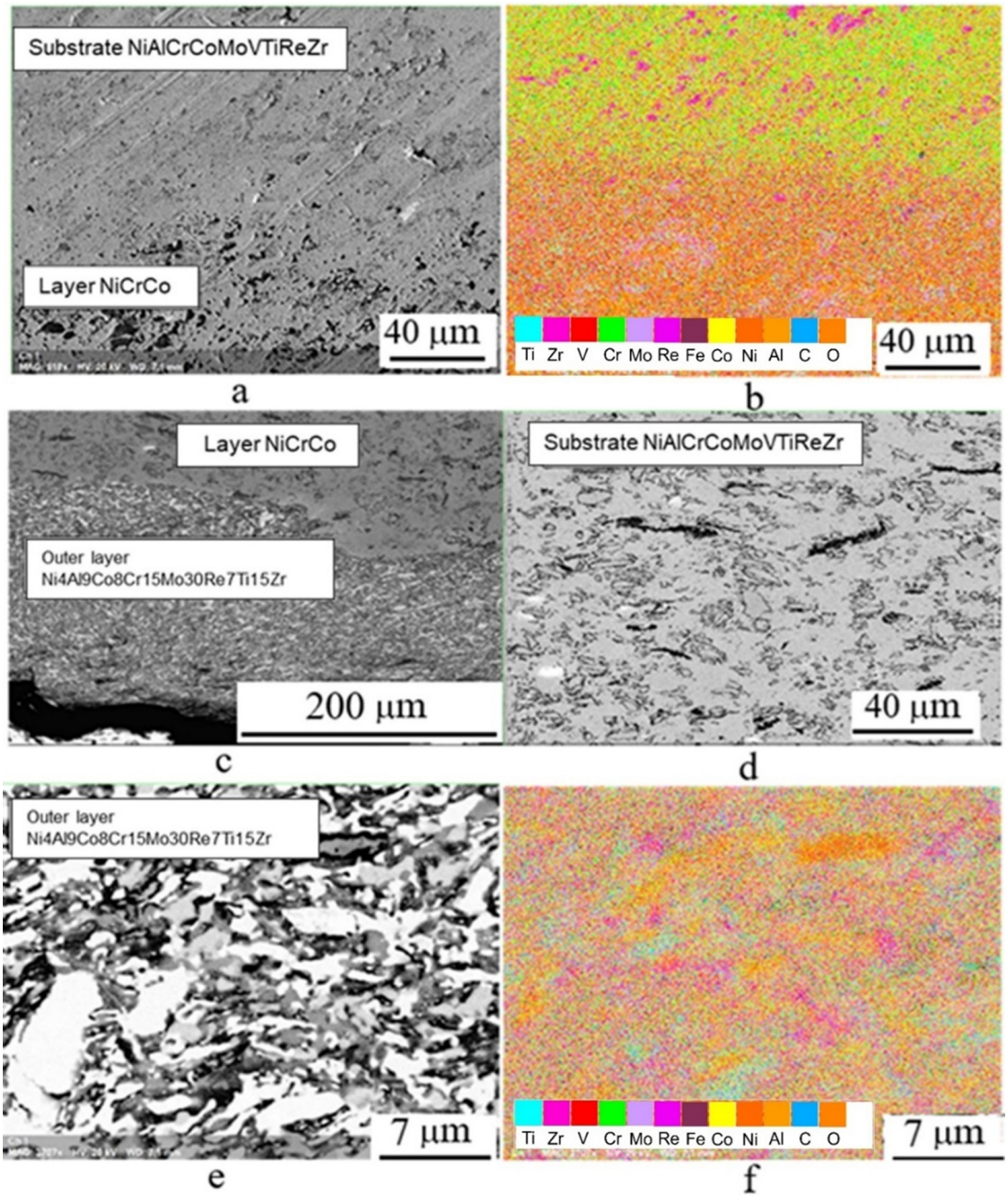

Figure 3 (a) SEM images of the cross-sectional structure of material 3 and (b) the element distribution map; (c) cross-sectional structure of material 4 and (d) its substrate and outer layer and (e) the element distribution map

According to the calculation of the isothermal cutoff at 1170 °C (sintering temperature) of the Re-Cr-Mo ternary diagram, the system contains a σ-phase, as well as a BCC solid solution mixed with at the considered element concentrations. According to the calculation of the Ni-Ti-Al diagram isothermal cutoff, the system also contains FCC, HCP, and BCC phases at the sintering temperature, as well as intermetallic compounds Ni3Ti, Al3Ni, NiAl, and others. According to the calculation of the isothermal cutoff of the Ni-Ti-Zr ternary diagram at 1170 °C, the material may contain a BCC solid solution and intermetallic compounds with zirconium, titanium, and nickel.

3.2 Electrochemical analysis and corrosion studies

From the physical production principles, composite materials are complex electrochemical systems consisting of numerous electrically small interconnected galvanic cells. This is the fundamental difference from "traditional" alloys produced by metallurgical methods (from a melt). Polarization curves were also obtained for "pure" metals in an aqueous solution of 25 g/l CsCl + 11 g/l KCl + 9 g/l NaCl to correlate the influence of individual alloying components on the electrochemical conductivity. These metals represent the main alloy components, such as nickel, chromium, and aluminum, as well as iron, which is an impurity (from 1 to 4 at.%). The corrosion potentials of the single-layer composites 1 and 2 are located between the corrosion potentials of pure aluminum (characterized by the most negative values), chromium (with intermediate values), and nickel (with the most positive potential values) (Figure 4). This indirectly indicates that nickel has greater thermodynamic stability in this environment than chromium and aluminum. The anodic polarization curve shows that aluminum is not passivated in this environment. A sharp increase in the anodic current values is observed when more positive values are shifted. Despite having a more negative corrosion potential than nickel, chromium has a longer passive region and low currents in the passivation potential range (i_{pp}). Nickel has a pronounced passive region in the potential range of 0–0.3 V. Then, a sharp increase in the current is observed. Based on the results of pure aluminum and iron, it should be assumed that their degradation influences the passivation properties of composites and, most likely, their corrosion resistance. This effect should be more significant than that of traditional alloys because composites are a set of mechanically and electrically interconnected galvanic cells. Other components, such as cobalt, molybdenum, vanadium, and titanium, can either improve or neutralize the corrosion resistance of composites. Therefore, nickel and chromium should reduce the corrosion rate of composites. Reducing the content of iron and aluminum is advisable because they reduce corrosion resistance.

The corrosion potential is more positive for the base material 1 (Figure 5). The i_{pp} currents are lower by half an order of magnitude presumably because of the presence of phase regions enriched in Al, Zr, and Ti in material 2. On the other hand, single-layer material 2 has a more extended passive state region than material 1 based on the anodic polarization curves. EDX mapping and X-ray phase analysis show the absence of individual phase regions of aluminum, and NiAl is one of the main phases of the material. As indicated by Xu et al., 2002, NiAl-based alloys form a higher-quality oxide film and are more resistant to corrosion in various environments than superalloys.

Fe^{3+} cations degrade the quality of the protective film. However, the formation of intermetallic compounds, including those based on Al and various other alloying additives, creates electrochemical heterogeneity in the material. The Ni/Al ratio for material 2 increased, the Ni/Cr ratio remained unchanged, the iron impurity content decreased, and the Mo and Co contents also increased. Titanium could positively affect the electrochemical behavior of material 2. The addition of titanium reduces the potential difference between the Al-Ni-rich phase and the Fe-Cr-rich phase, weakening the galvanic effect or selectively dissolving the alloy.

The formation of additional layers on the matrix surface corresponding to material 2 "shifts" the corrosion potential for material 3. It is apparently due to a significant reduction in the surface layer aluminum content. However, in the case of the two-layer structure (NiAl-

NiCrCoTiMoVReZr substrate–NiCrCo layer), the passive region became less extensive (Figure 5). Moreover, the Ni/Cr ratio is significantly increased, contributing to the positive shift in the potential but resulting in a less extensive passive region than for single-layer materials.

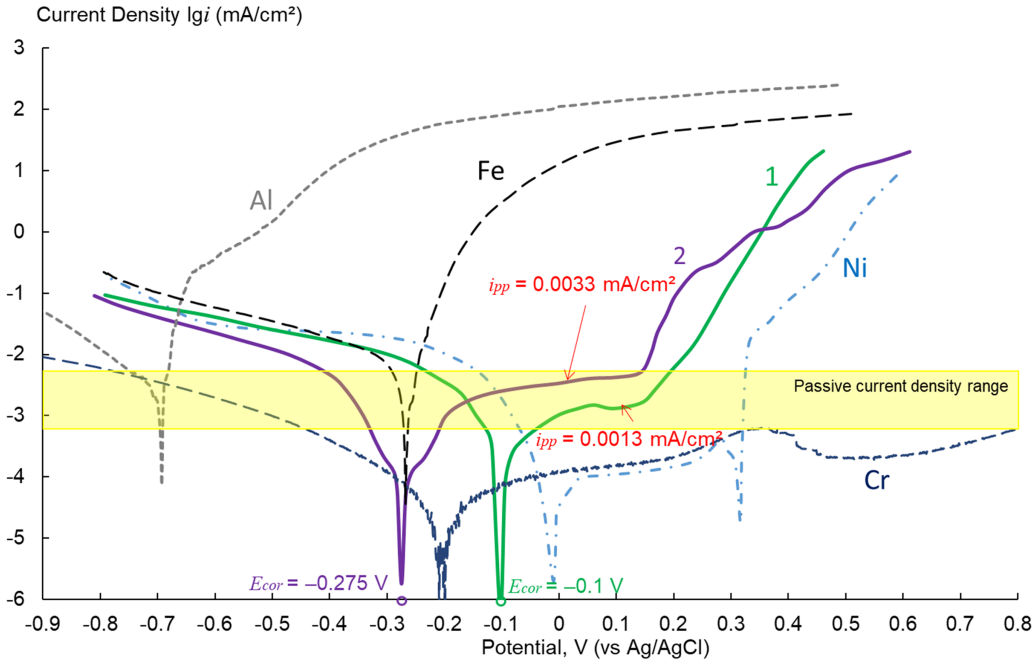

Figure 4 Polarization curves of single-layer composites (1 base, 2) and pure metals (Al, Fe, Ni, Cr) in a solution of 25 g/l CsCl + 11 g/l KCl + 9 g/l NaCl

An additional upper layer of Ni4Al9Co8Cr15Mo30Re7Ti15Zr (wt.%) was added to material 3 when material 4 was formed. The addition of this layer slightly shifts the corrosion potential toward the negative side. This may be due to the increased aluminum content and decreased Ni/Cr ratio. Simultaneously, the passive region significantly increases, and the anodic current decreases by approximately half a magnitude compared to sample 2.

The corrosion potential values Ecor of materials 1, 3, and 4 are close to each other, except for alloy 2 (Figure 6). Its corrosion potential is the most negative, but it has the longest passive region, 415 mV, which can be considered a positive factor. Simultaneously, the highest current density was observed in the passive state (0.0033 versus 0.0013-0.0015 mA/cm^2 for the other alloys). Thus, the multilayer material NiAlNiCrCoMoVReTiZr/NiCrCo/NiAlCoCrMoReTiZr has demonstrated the most optimal characteristics in terms of the ratio of current density in the passive state and the extent of the passive state region, 299 mV and 0.0014 mA/cm^2, indicating its greater corrosion resistance in the used environment.

Corrosion in an aqueous chloride solution (25 g/L CsCl + 11 g/L KCl + 9 g/L NaCl) is a classic example of electrochemical corrosion. Aggressive chloride ions (Cl^-) are capable of destroying protective passive oxide films on the surface of metals, leading to localized forms of destruction, such as pitting and crevice corrosion. Corrosion tests showed no changes in the mass of the obtained materials after exposure to this solution for 6 months. Areas of an oxide-chloride film were formed only on the surface of material 1 (Figure 7). Its composition according to EDX data is as follows: Cs, 21.7 at.%; Cl, 36.7 at.%; Na, 13.0 at.%; and O, 28.6 at.%. No traces of pitting damage were detected after either corrosion or electrochemical studies. This may be due to the chemical composition of NiAl-based alloys, the presence of regions with a high-entropy structure, and the formation of intermetallic compounds that enhance corrosion resistance.

A complex combination of electrochemical and metallurgical factors determines the corrosion resistance of multicomponent nickel composites in chloride solutions. The alloying elements play a key role in resisting this process. Cr is the main element providing passivation, as shown in

Figure 4. At a Cr content of more than 13%, it forms a dense and continuous layer of chromium oxide (Cr_2O_3) on the surface, which isolates the metal from the corrosive environment. An increase in the Cr content increases the stability of the passive film, as was found in previous studies (Henderson et al., 2020; Ebrahimi et al., 2017). At the same time, Mo increases the resistance of the alloy to pitting corrosion in chloride-containing environments and strengthens the passive film, preventing its local destruction (Henderson et al., 2021; Zadorozne et al., 2010). The Ni-Cr-Mo alloy is known for their exceptional corrosion resistance in aggressive oxidizing environments, such as chloride melts. Although Al can also form a protective oxide film, when incorporated into complex alloys and in contact with more "noble" metals (e.g., nickel), Al can act as an anode in a galvanic couple and undergo preferential dissolution. A low aluminum content (approximately 1.25%) promotes an increase in the chromium oxide content in the passive layer (Kositsyn and Kositsyna, 2008). Moreover, the enrichment of the surface with a more corrosion-resistant component is possible during the corrosion process due to the selective dissolution of the less corrosion-resistant component. Wu et al., 2022 noted that the addition of Ti can improve the corrosion resistance, particularly the pitting resistance, of the AlCrFeCoNi alloy, which is reflected in a decrease in i_{corr} and i_{pit}. It is also associated with the formation of more protective passive films that prevent the transfer of point defects and the destruction of the passive film.

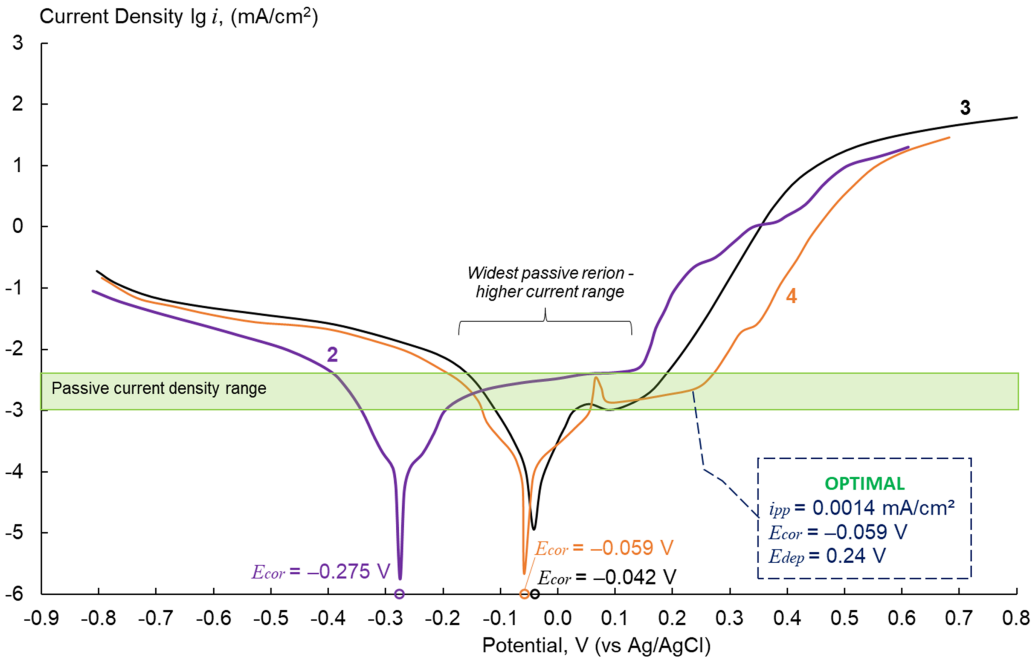

Figure 5 Polarization curves of the two-layer 3 and three-layer 4 materials relative to the single-layer material 2 (substrate) in a solution of 25 g/l CsCl + 11 g/l KCl + 9 g/l NaCl

This complex interplay of alloying elements is particularly critical for NiAl-based materials. Their behavior in chlorides is highly dependent on the material form and environmental conditions. For instance, while plasma-sprayed Ni-Al coatings showed better performance in 3.5% NaCl (icorr of 19 $\mu A/cm^2$) than in 0.01 M H_2SO_4 (28 $\mu A/cm^2$) (Starosta, 2013), electrodeposited Ni-Al composite coatings exhibited a 25-fold higher corrosion current density (5.057 $\mu A/cm^2$) compared to pure nickel in 2 M NaCl (Onyeachu et al., 2017). This increased activity in the composite was attributed to Al particle-induced porosity, which created charge percolation pathways and increased the active surface area (Onyeachu et al., 2017).

Furthermore, the stability of the protective Al_2O_3 layer is strongly dependent on chloride concentration and pH. Protective Al_2O_3-enriched layers can develop at moderate chloride concentration ($\leq$ 0.6 M NaCl) within a pH range of 4-9 (Onyeachu et al., 2015). However, at higher

concentrations (≥ 2 M NaCl), chlorides prevent stable passivation by consuming Al corrosion products to form soluble complexes, leading to localized corrosion layer collapse (Onyeachu et al., 2017). This is consistent with observations on single-crystal NiAl, where exposure to 0.5 M NaCl led to progressive chloride penetration and the formation of mixed Ni-Al chloride-hydroxide species after more than 20 h, indicating a loss of protection (Bennour et al., 2010).

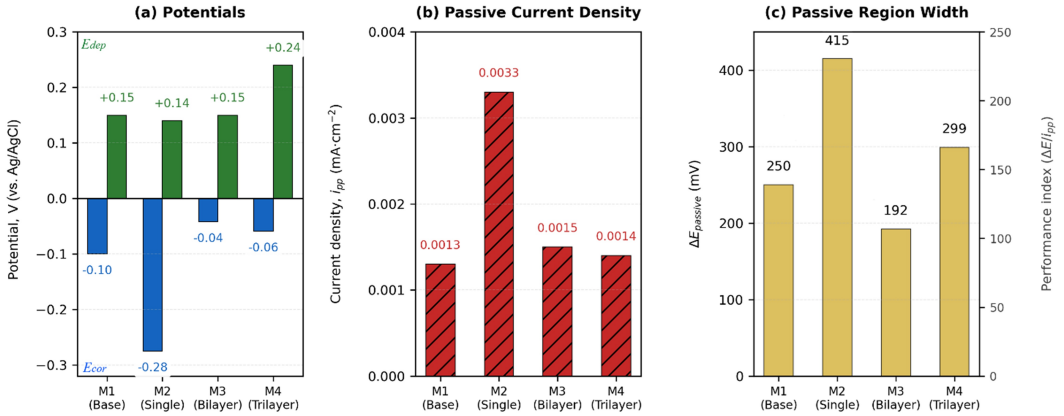

Figure 6 (a) Corrosion potential (E_{cor}) and depassivation potential (Edep) (a), passive state current density (ipp) (b), passive region width (c)

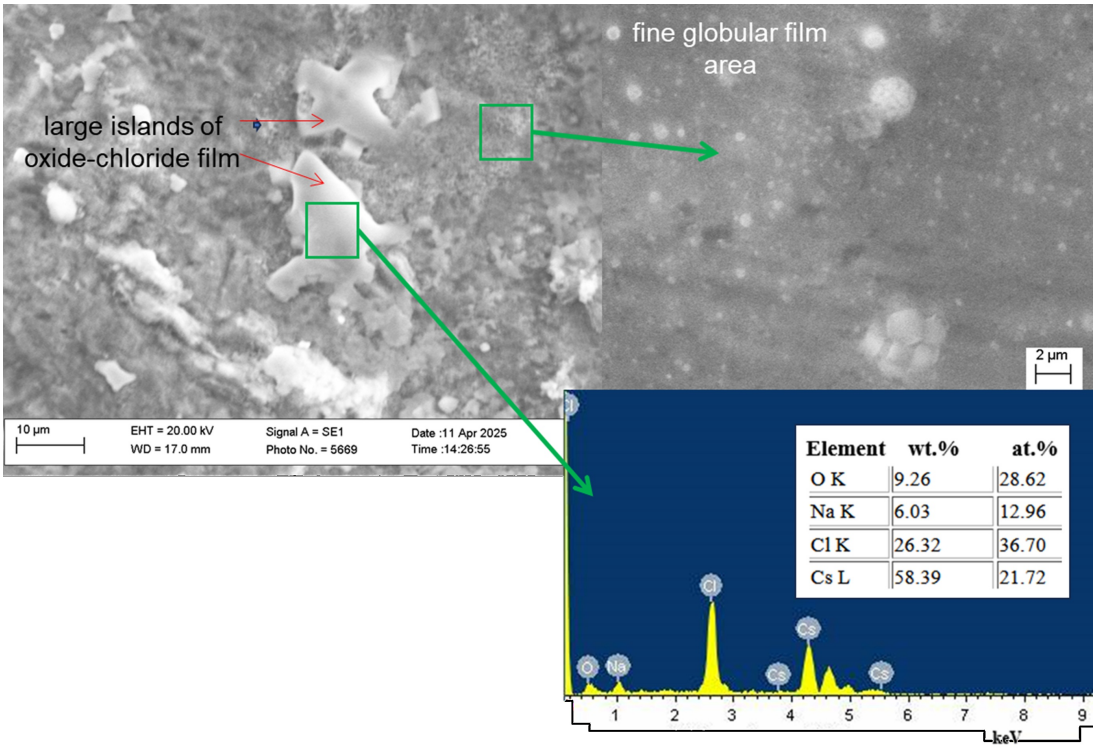

Figure 7 Microstructure of composite 1 after corrosion testing for 6 months in a solution of 25 g/l CsCl + 11 g/l KCl + 9 g/l NaCl

Material 4, with a high molybdenum content and alloyed with chromium and titanium, has the greatest potential for corrosion resistance in an aggressive chloride environment. The formation of a high-quality passive film ensures this resistance, where chromium forms a barrier and molybdenum promotes its restoration at sites of localized damage (Romanovskaia et al., 2022). Molybdenum cations are incorporated into the oxide layer, significantly enhancing its protective properties. The superior performance of this material can be contextualized by the literature: its high Mo content is critical for resisting pitting in chlorides (Zadorozne et al.,

2010), while the combined Cr and Ti contribution aids in forming a more protective passive film (Wu et al., 2022). Alloyed NiAl materials can exhibit higher pitting and passivation potentials than conventional materials, such as 316L stainless steel (Colin et al., 2007); this indicates a strong inherent potential that material 4 successfully realizes. Other metallurgical factors, such as solid solution homogeneity, fine-grain structure, and low dislocation density, are also important for corrosion resistance against localized types (Kositsyn and Kositsyna, 2008). The long-term aging of passive films leads to their enrichment in chromium and "washing out" of nickel, which increases the regeneration ability of the material (Romanovskaia et al., 2024). This time-dependent improvement is consistent with observations for Ni-Al composites in 3.5% NaCl, where prolonged immersion (up to 72 h) led to Al_2O_3 enrichment of the corrosion layer, reducing the corrosion rate and pitting susceptibility (Onyeachu et al., 2015). These trends align with recent HEA corrosion reviews emphasizing multi-principal chemistries, sluggish diffusion, and defect-tolerant passivity in chloride-bearing media (George et al., 2019; Shi et al., 2017; Tsai and Yeh, 2014).

Figure 8 presents an integrated correlation between the architectural hierarchy (single-, bi-, and trilayer configurations), phase composition (FCC/BCC matrices containing B2 NiAl intermetallics and σ/μ TCP phases), and electrochemical performance of the developed composites. The summary diagram clearly maps the progression from simple to gradient multilayer structures against polarization metrics, highlighting the trilayer Material 4 as the optimal system with the widest passive region (299 mV) and minimized passive current density (0.0014 mA/cm^2).

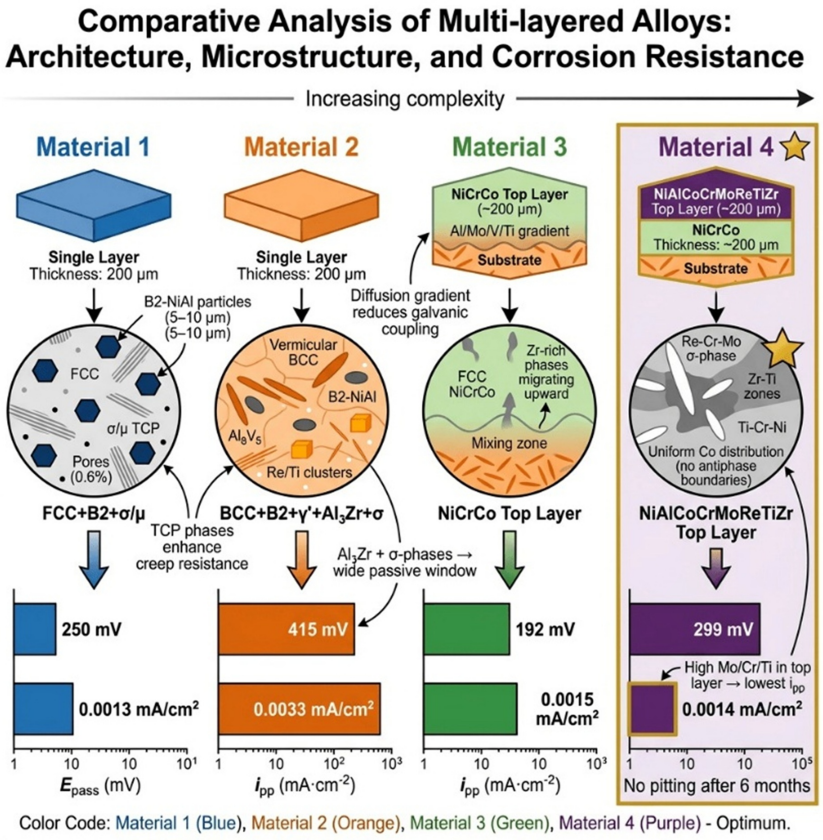

Figure 8 Integrated correlation of material architecture, electrochemical performance, and corrosion stability

The annotated potentiodynamic curves distinctly separate the pure metal references (dashed lines) from the composite responses (solid lines), with shaded passive regions and marked critical potentials (Ecor, Erep) facilitating immediate visual interpretation. Post-corrosion microanalysis confirmed the absence of pitting across all compositions after six months of exposure, with Material 4 exhibiting the most uniform protective film formation. Collectively, these data

demonstrate that strategic architectural complexity and high-entropy multicomponent design synergistically enhance corrosion resistance in aggressive chloride environments.

4. Conclusions

NiAl-based composite materials with single-layer (NiAl-CrMoCoV, NiAl-NiCrCoMoVReTiZr), bilayer (NiAl-NiCrCoMoVReTiZr/NiCrCo), and trilayer (NiAl-NiCrCoMoVReTiZr/NiCrCo/NiAlCoCrMoReTiZr) structures were produced by spark plasma sintering. The materials comprise a matrix of FCC solid solution and regions with a mixed FCC-BCC structure containing large particles of the NiAl-based B2 intermetallic compound. Lamellar phases interspersed with nanoscale and submicron spherical phase clusters were observed. Solid solutions of BCC, FCC, and NiAl are present, as well as TCP σ- and μ-phases based on the Cr-Mo system. Electrochemical studies in an aqueous solution (25 g/l CsCl + 11 g/l KCl + 9 g/l NaCl) revealed that the single-layer NiAl-NiCrCoMoVReTiZr material has the longest passive state region. However, it exhibits the highest current density in the passive state, 0.0033 mA/cm2 versus 0.0013-0.0015 mA/cm2 for the other alloys, as well as the most negative corrosion potential. The lowest passive currents were obtained for the NiAl-CrMoCoV material. The three-layer NiAl-NiCrCoMoVReTiZr/NiCrCo/NiAlCoCrMoReTiZr material exhibited the most optimal values in terms of the ratio of passive current density to passive region length at 299 mV and 0.0014 mA/cm^2. This demonstrates its superior corrosion resistance in this environment due to the formation of a high-quality passive film, ensured by the high molybdenum, chromium, and titanium content of the material. Corrosion studies performed after aging for 6 months revealed no changes in mass or traces of pitting in the material structure. This may be due to both the chemical composition of NiAl-based alloys and the presence of regions with a high-entropy structure and intermetallic compounds that enhance corrosion resistance.

Acknowledgements

The Ministry of Education and Science of Russia supported this work, Grant No. FSFF-2023-0006. The authors would like to thank the staff of JSC "Keldysh Research Center", the Head of the Department of Nanotechnologies of JSC "Keldysh Research Center" R. N. Rizakhanov, Professor of the Department of PMFP at NUST "MISIS" V. I. Kostikov, and Associate Professor of the Department of PMFP at NUST "MISIS" Zh. V. Eremeeva for their cooperation and valuable consultations.

Author Contributions

Conceptualization, L.A. and S.S.; methodology, S.S. and M.G.; software, L.A. and V.I.; validation, L.A., S.S. and V.I.; formal analysis, A.A.; investigation, L.A.; resources, L.A and V.I..; data curation, L.A. and M.G.; writing—original draft preparation, L.A. and M.G.; writing—review and editing, S.S.; visualization, L.A. and M.G.; supervision, L.A.; project administration, L.A.; funding acquisition, L.A. All authors have read and agreed to the published version of the manuscript.

Conflict of Interest

The authors declare no conflicts of interest.

Declaration of AI

There is no artificial intelligence generated content in this text.

References

Agureev, L., Kostikov, V., Savushkina, S., Eremeeva, Z., & Lyakhovetsky, M. (2022). Preparation and study of composite materials of the NiAl-Cr-Mo-Nanoparticles (ZrO2, MgAl2O4) system. *Materials*, *15*(17), 5822. https://doi.org/10.3390/ma15175822

Agureev, L., Savushkina, S., Danilina, E., Ivanova, S., Ivanov, A., & Garibashvili, S. (2025). Preparation and study of the sintered NiAl-CrMoCoV equiatomic system composite material structure and properties. *Journal of Materials Engineering and Performance*, *34*, 26324–26338. https://doi.org/10.1007/s11665-025-11255-w

Beneš, O., Capelli, E., Morelová, N., Colle, J.-Y., Tosolin, A., Wiss, T., Cremer, B., & Koning, R. (2021). Cesium and iodine release from fluoride-based molten salt reactor fuel. *Physical Chemistry Chemical Physics*, *23*, 9512–9523. https://doi.org/10.1039/D0CP05794K

Bennour, I., Maurice, V., & Marcus, P. (2010). X-ray photoelectron spectroscopy study of the interaction of ultra-thin alumina films on NiAl alloys with NaCl solutions. *Surface and Interface Analysis*, *42*(6–7), 581–587. https://doi.org/10.1002/sia.3168

Colin, J., Serna, S., Campillo, B., et al. (2007). Corrosion performance of a rapidly solidified NiAl intermetallic macroalloyed with Fe in 0.5m H2SO4. *International Journal of Electrochemical Science*, *2*(12), 947–957. https://doi.org/10.1016/s1452-3981(23)17125-2

Dikici, B., Lindner, T., Sakar, E., Lampke, T., Seifzadehd, D., Grund, T., & Kamacı, K. (2025). Enhancing corrosion resistance and radiation shielding of AISI 304 SS with Nb and Mo-added Al0.3CrFeCoNi-based high-entropy alloy coatings in 3.5 wt% NaCl: The effect of environmental temperature. *Journal of Alloys and Compounds*, *1020*, 179432. https://doi.org/10.1016/j.jallcom.2025.179432

Ebrahimi, N., Biesinger, M., Shoesmith, D., & Noël, J. (2017). The influence of chromium and molybdenum on the repassivation of nickel-chromium-molybdenum alloys in saline solutions. *Surface and Interface Analysis*, *49*, 297–308. https://doi.org/10.1002/sia.6254

Farihin, P., Suharno, B., Aziz, F., Dani, M., Ngarayana, I., Andryansyah, Insani, A., Wardana, R., Adhika, D., & Huang, C. (2025). High-resolution neutron diffraction analysis of residual stresses in oxide dispersion strengthened FeNiCrY2O3 cast alloys for advanced nuclear reactor applications. *International Journal of Technology*, *16*(2), 625–638. https://doi.org/10.14716/ijtech.v16i2.7241

Feng, J., Ye, X., Lei, H., Chen, J., Diao, Z., Zhao, G., Li, B., & Fang, D. (2024). Effect of synergistic alloying of Co and Mo on solidification microstructure and properties of NiAl-based eutectic high-entropy alloy. *Journal of Materials Engineering and Performance*, *33*, 12765–12771. https://doi.org/10.1007/s11665-023-08868-4

Fu, H., Hou, Z., Fu, J., & Ma, Y. (2013). Elastic anisotropy and phonon focusing in NiAl: Atomic study. *Intermetallics*, *42*, 156–164. https://doi.org/10.1016/j.intermet.2013.06.005

George, E. P., Curtin, W. A., & Tasan, C. C. (2019). High-entropy alloys. *Nature Reviews Materials*, *4*, 515–534. https://doi.org/10.1038/s41578-019-0121-4

Grachev, V., Rozen, A., Perelygin, Y., Kireev, S., & Los, I. (2020). Multilayer corrosion-resistant material based on iron-carbon alloys. *Heliyon*, *6*, e04039. https://doi.org/10.1016/j.heliyon.2020.e04039

He, H., Liu, C., He, L., Wang, G., Zhang, W., Zhao, S., Xiang, Y., & Yi, J. (2023). Microstructure, mechanical properties and high temperature corrosion of [AlTiCrNiTa/(AlTiCrNiTa)N] high entropy alloy multilayer coatings for nuclear fuel cladding. *Vacuum*, *212*, 112057. https://doi.org/10.1016/j.vacuum.2023.112057

Henderson, J. D., Almusned, B., Momeni, M., Anderson, S., Dehnavi, V., Zagidulin, D., Shoesmith, D., & Noël, J. J. (2020). Investigating the influence of Cr and Mo additions to commercial Ni-based alloys exposed to neutral and acidic chloride solutions. *Journal of the Electrochemical Society*, *167*, 131512. https://doi.org/10.1149/1945-7111/abbea7

Henderson, J. D., Li, X., Filice, F., Zagidulin, D., Biesinger, M., Kobe, B., Shoesmith, D., Ogle, K., & Noël, J. (2021). Investigating the role of Mo and Cr during the activation and

passivation of Ni-based alloys in acidic chloride solution. *Journal of The Electrochemical Society*, *168*, 021506. https://doi.org/10.1149/1945-7111/abe47a

Jiang, Y., Li, S., Huang, D., Bao, Z., Wang, J., Zhu, S., & Wang, F. (2025). Unveiling corrosion reaction mechanism of β-NiAl coating modified by platinum and hafnium in NaCl- or Na2SO4-containing mediums. *Journal of Materials Science & Technology*, *237*, 54–67. https://doi.org/10.1016/j.jmst.2025.01.077

Kositsyn, V., & Kositsyna, I. (2008). Phase and structural transformations in the alloys based on monoaluminide of nickel. *Progress in Physics of Metals*, *9*(2), 195–258. https://doi.org/10.15407/ufm.09.02.195

Lambrecht, M., García-Martín, G., Miguel, M., Lasanta, M., & Pérez, F. (2022). Corrosion study of Ni-based alloy in ternary chloride salt for thermal storage application. *Corrosion Science*, *208*, 110673. https://doi.org/10.1016/j.corsci.2022.110673

Lian, C., Xie, W., Fang, H., Wang, W., Yu, J., Li, J., & He, X. (2025). Effect of Cr:Al ratio on corrosion mechanism of Ni-Cr-Mo-Al alloys in 3.5 wt.% NaCl solution: Microstructure and electrochemical and passive characteristics. *Materials*, *18*(10), 2177. https://doi.org/10.3390/ma18102177

Minamino, Y., Koizumi, Y., Tsuji, N., Morioka, M., Hirao, K., & Shirai, Y. (2000). Pt diffusion in B2-type ordered NiAl intermetallic compound and its diffusion mechanisms. *Science and Technology of Advanced Materials*, *1*(4), 237–249. https://doi.org/10.1016/S1468-6996(01)00003-1

Müller, M., Heinen, B., Riede, M., López, E., Brückner, F., & Leyens, C. (2021). Additive manufacturing of β-NiAl by means of laser metal deposition of pre-alloyed and elemental powders. *Materials*, *14*(9), 2246. https://doi.org/10.3390/ma14092246

Onyeachu, B., Peng, X., Oguzie, E., et al. (2015). Characterizing the electrochemical corrosion behaviour of a Ni–28 wt.% Al composite coating in 3.5% NaCl solution. *Portugaliae Electrochimica Acta*, *33*(2), 69–83. https://doi.org/10.4152/pea.pea.201502069

Onyeachu, I., Njoku, D., Oguzie, E., & Peng, X. (2017). Corrosion of a Ni-Al composite coating in 2 m NaCl solution. *Portugaliae Electrochimica Acta*, *35*(3), 179–186. https://doi.org/10.4152/PEA.201703179

Perelygin, Y., Rosen, A., Los, I., & Kireev, S. (2014). A new corrosion-resistant multilayer material. *Protection of Metals and Physical Chemistry of Surfaces*, *50*(7), 856–859. https://doi.org/10.1134/S2070205114070132

Povarova, K., Bazyleva, O., Drozdov, A., Morozov, A., Antonova, A., Sirotinkin, V., Bulakhtina, M., Arginbaeva, E., & Alad'ev, N. (2019). High-temperature β-NiAl + γ'-Ni3Al + γ-Ni alloys of the Ni–Al–Co system. *Russian Metallurgy (Metally)*, *2019*(11), 1167–1177. https://doi.org/10.1134/S0036029519110089

Rao, S. G., Shu, R., Wang, J., Chai, J., Zhu, Y., le Febvrier, A., & Eklund, P. (2024). Mechanical properties of Xe-ion-irradiated high-entropy-alloy-based multilayers. *Applied Physics Letters*, *124*(6), 061906. https://doi.org/10.1063/5.0187142

Rizkia, V., Munir, B., Soedarsono, J., & Suharno, B. (2015). Corrosion resistance enhancement of an anodic layer on an aluminum matrix composite by cerium sealing. *International Journal of Technology*, *6*(7), 1191–1197. https://doi.org/10.14716/ijtech.v6i7.1260

Romanovskaia, E., Lutton, K., Amalraj, M., Marks, L., & Scully, J. (2022). Formation and long-time exposure aging of oxides on Ni-Cr and Ni-Cr-X (Mo, W) alloys in acidic chloride solutions: Ramifications towards local corrosion resistance. *ECS Meeting Abstracts*, *MA2022-02*(11), 711. https://doi.org/10.1149/MA2022-0211711mtgabs

Romanovskaia, E., Lutton, K., Marshal, A., Wang, K., Chan, H., Zhou, B., & Scully, J. (2024). Formation and long-time exposure aging of oxides on Ni-Cr and Ni-Cr-X (X = Mo, W) alloys in acidic chloride solutions: Ramifications towards corrosion resistance. *Applied Surface Science*, *661*, 159998. https://doi.org/10.1016/j.apsusc.2024.159998

Sasi, A., Vikram, R. J., & Dash, K. (2025). Corrosion and oxidation behavior of high entropy alloys in extreme and harsh environments: A perspective on steam corrosion. *Journal of Applied Physics*, *138*(2), 020701. https://doi.org/10.1063/5.0273671

Shi, Y., Yang, B., & Liaw, P. K. (2017). Corrosion-resistant high-entropy alloys: A review. *Corrosion Science*, *119*, 33–45. https://doi.org/10.3390/met7020043

Starosta, R. (2013). Corrosion of Ni-Al and Ni-Al-Al2O3 plasma sprayed coatings in 0.01 m H2SO4 and 3.5% NaCl solutions. *Solid State Phenomena*, *199*, 390–395. https://doi.org/10.4028/www.scientific.net/SSP.199.390

Sun, L., Ye, X., Diao, Z., Yang, J., Xia, D., Wu, G., Kang, H., Zhao, G., Li, B., & Fang, D. (2025). Microstructure, mechanical and corrosion properties of (CoCrFeNi)82-x(NiAl)18Nbx triple-phase high-entropy alloys. *Materials Science & Engineering A*, *948*, 149301. https://doi.org/10.1016/j.msea.2025.149301

Tsai, M.-H., & Yeh, J.-W. (2014). High-entropy alloys: A critical review. *Materials Research Letters*, *2*(3), 107–123. https://doi.org/10.1080/21663831.2014.912690

Wang, Y., Jiang, Y., Yu, C., Sun, L., & Li, Y. (2014). First-principles study of elastic properties of NiAl doped with transition elements. *Computational Materials Science*, *95*, 420–426. https://doi.org/10.1016/j.commatsci.2014.07.060

Wu, M., Setiawan, R. C., & Li, D. Y. (2022). Benefits of passive element Ti to the resistance of AlCrFeCoNi high-entropy alloy to corrosion and corrosive wear. *Wear*, *492–493*, 204231. https://doi.org/10.1016/j.wear.2021.204231

Xu, S., Zhu, Y., Huang, X., Zhou, B., & Yu, Z. (2002). Corrosion resistance of the intermetallic compound, NiAl, in a molten carbonate fuel cell environment. *Journal of Power Sources*, *103*(2), 230–236. https://doi.org/10.1016/S0378-7753(01)00854-0

Zadorozne, N. S., Rodríguez, M., Carranza, R., Meck, N. S., & Rebak, R. (2010). Corrosion resistance of Ni-Cr-Mo and Ni-Mo-Cr alloys in different metallurgical conditions. *Proceedings of the CORROSION 2010*, 1–32. https://doi.org/10.5006/C2010-10236

Zhang, W., Tang, R., Yang, Z., Liu, C., Chang, H., Yang, J., Liao, J., Yang, Y., & Liu, N. (2018). Preparation, structure, and properties of high-entropy alloy multilayer coatings for nuclear fuel cladding: A case study of AlCrMoNbZr/(AlCrMoNbZr)N. *Journal of Nuclear Materials*, *512*, 15–24. https://doi.org/10.1016/j.jnucmat.2018.10.001